Development of a Real-time Latching Control Algorithm Based on Wave Force Prediction

Liang Li, Hongdong Wang*, and Yan Gao

***Abstract*—Optimal wave energy control is non-causal as the control command is optimized based on incoming wave force. Therefore, implementation of wave energy control requires forecasting of future wave force. A real-time latching control algorithm based on short-term wave force prediction is developed in this study to tackle such non-causality. The future wave forces are forecasted using the grey model. The receding horizon strategy is used to optimize the control command online and over the prediction horizon interval. Based on the predicted wave forces, the power extraction is maximized by locking and releasing the buoy alternately according to the optimized control command. Simulation results show that the power extraction is increased substantially with implementation of the developed real-time latching control algorithm, even if the future wave forces are predicted. Effects of prediction length and prediction error on the energy conversion are examined. It is found that more wave energy is harvested when a long prediction length is employed whilst prediction error decreases the control efficiency. The extreme load of power take-off system increases when the wave energy control is implemented although its travel distance is hardly varied.**

***Index Terms*— wave energy converter; energy maximization; latching control; wave force prediction; extreme response**

L. Li and Y. Gao are with Department of Naval Architecture, Ocean and Marine Engineering, University of Strathclyde, UK (e-mail: liang.li@strath.ac.uk; yan.gao@strath.ac.uk). L. Li is with State Key Laboratory of Hydraulic Engineering Simulation and Safety, Tianjin University, PR China. Y. Gao is with State Key Laboratory of State Key Laboratory of Coastal and Offshore Engineering, Dalian University of Technology, PR China.

H. Wang (corresponding author) is with MOE Key Laboratory of Marine Intelligent Equipment and System, Shanghai Jiao Tong University, PR China. (e-mail: whd302@sjtu.edu.cn).

I. INTRODUCTION

It is expected that the global demand for energy will climb up to 25 percent by 2040 and the world is pursuing economic and renewable energy sources to keep up with this considerable demand growth [1]. Compared with other ocean energy resources, wave energy is a kind of resource with high power density and all-day availability. Due to these advantages, wave energy is regarded as a prospective solution to the sustainable generation of power. Various types of wave energy converters have been developed to harvest energy from ocean waves. Li et al. [2] showed the power output of an oscillating-body WEC installed on a spar-type floating wind turbine. Sheng and Lewis [3] optimized the power take-off (PTO) system of oscillating water column WECs.

Despite the developments of WECs with various energy conversion mechanisms, the energy harvesting efficiency is still not satisfactory, especially in random waves. An effective approach to enlarge the energy absorption is the implementation of wave energy control. The latching control was firstly introduced by Budal and Falnes [4]. They maximized the power extraction by locking and releasing the buoy alternately to keep the buoy velocity in phase with the wave excitation force. In this way, resonance could be achieved. Babarit and Clement [5] assessed the power extraction of an oscillating-body WEC with latching control. Based on the pre-generated wave elevations, the optimal command theory was applied to determine the control command offline. A similar approach was adopted by Henriques et al. [6] to increase the power extraction of an oscillating-water-column WEC. The sensitivity of energy absorption to receding horizon length was examined. Babarit et al. [7] compared different latching control strategies of a WEC in the random sea. When the control strategy was designed to maximize different variables (magnitude of motion, magnitude of velocity, etc.), the performance of the WEC showed discrepancies.

The latching control is non-causal, which optimizes the control command based on future wave excitation force. Previously studies on the latching control generally assumed that the coming wave force was already known whereas the information of future wave force is unknown in the real world. Consequently, it is necessary to predict the future wave force to implement the latching control practically.

The wave force prediction approaches can be briefly classified into two categories. The first group is the spatial prediction, which forecasts the wave information at a certain point based on the observations at nearby locations. The second group predicts sea waves with the collection of past wave information right at this point and thereby no other quantities are required. This approach is essentially a random signal processing technology and does not need the dynamic model of the random process. Consequently, it applies to the prediction of many variables, such as wave elevation, wave force, floater velocity, etc. Halliday et al. [8] utilized the fast Fourier transformation to predict random sea waves. A wave prediction model based on the grey model was developed by Truong and Ahn [9]. Other wave force prediction approaches include the autoregressive model and the orthogonal basis function, etc. The wave force prediction technology has been used to tackle the non-causality of several other wave energy control algorithms. Fusco and Ringwood [10] utilized the linear autoregressive model for the practical implementation of the non-causal reactive control. Schoen et al. [11] include the wave force prediction in their fuzzy logic controller. Li et al. [12] applied the so-called bang-bang control with consideration of the wave force prediction. Nevertheless, the development of a latching control algorithm with wave force prediction is hardly reported and the sensitivity of the latching control to the wave force prediction is not fully known.

The primary objective of this study is to develop a real-time latching control algorithm which incorporates a wave force prediction model. The energy capture performances with and without the predictive latching control algorithm are investigated under a set of sea states, where the information of future wave forces is forecasted. The efficiency of the control algorithm, the influences of and prediction length and error, and the control effect on the PTO dynamic response will be examined as well.

II. NUMERICAL MODELLING

The WEC considered in this study is a heaving point-absorber. As shown in Fig. 1, the floater is a hemisphere with a radius of 5 m and rigidly connected to the PTO system. The draft is 5 m at the equilibrium position. Only heave motion of the WEC is allowed. The PTO system is approximated by a linear springdamper system. According to Ref [13], the typical stiffness of a PTO system is around ten percent of the hydrostatic coefficient. Therefore, $K = 0.1\rho g\pi R^2$ is adopted. Fig. 2 illustrates the sensitivity of the PTO system to wave frequency ω and damping coefficient C. To harvest as much energy as possible, $C = 8.14\times10^5$ kg/s is used.

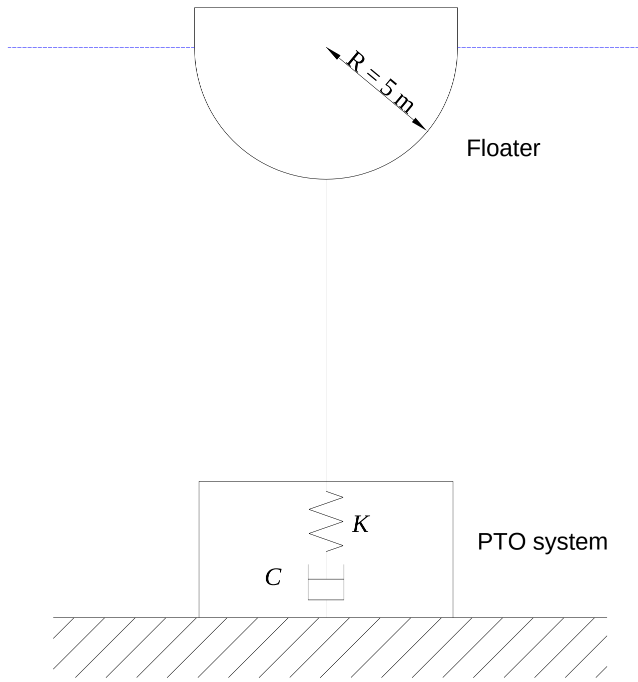

Fig. 1. Wave energy converter.

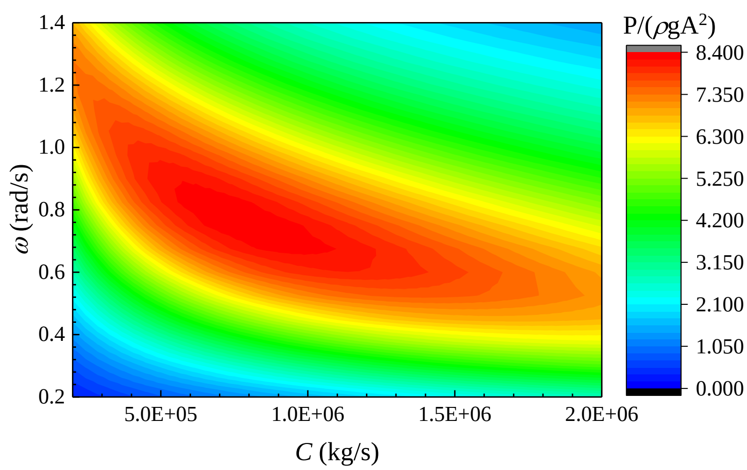

Fig. 2. The sensitivity of energy absorption to wave frequency and damping coefficient C in regular waves. Wave amplitude A = 1 m.

A. Dynamics of the WEC

The time-domain motion equation of the floater is given by

$$\left(M+m\right)\ddot{z}(t)+\int_{0}^{t}H(t-\tau)\dot{z}(\tau)d\tau+\rho g\pi R^{2}z(t)=F_{wave}(t)-C\dot{z}(t)-Kz(t)-\beta(t)c\dot{z}(t) \tag{1}$$

where M is the mass of the floater and m is the added mass at infinite frequency. z, $\dot{z}$, and $\ddot{z}$ are the displacement, the velocity, and the acceleration of the floater. W_{ave} is the wave excitation force. Latching control is used in the present study, and β(t) is the binary control command. When $\beta = 1$, the latching control is applied; when $\beta = 0$, it is not. c is a very large and finite value, representing the latching action. Following the suggestion of Henriques et al. [6], $c = 80(M+m)$ is employed in the present simulation. H is the so-called retardation kernel function which represents the memory effect of the free surface. It can be obtained either from the added mass $a(\omega)$ or the potential damping $b(\omega)$ [14]

$$H(t)=\frac{2}{\pi}\int_{0}^{\infty}\frac{a(\omega)}{\omega}\sin(\omega t)d\omega=\frac{2}{\pi}\int_{0}^{\infty}b(\omega)\cos(\omega t)d\omega \tag{2}$$

The Airy wave model is used to generate the stochastic wave elevations, which consist of multiple regular wave components with different oscillating frequencies and phases. Based on the Airy wave model, the wave forces are estimated by the linear transfer function

$$\begin{aligned}F_{wave}(t)&=\mathrm{Re}\left[\sum_{j=1}^{N}\Phi_{j}A_{j}e^{i(\omega_{j}t+\varepsilon_{j})}\right]\\A_{j}&=\sqrt{2S(\omega_{j})\Delta\omega}\end{aligned} \tag{3}$$

where A_j, ω_j, and ε_j are the wave amplitude, the frequency, and the random phase of regular wave component j. $S(\omega)$ is the wave spectrum. Φ_j is the linear wave force transfer function of wave component j.

B. *State-space representation*

Eq. (1) is widely used to simulate the dynamics of a floating body in the seakeeping problem. Nevertheless, it is inconvenient for the implementation of the control strategy and thereby a state-space representation is developed. Denote a dynamic system with input $x(t)$ and output $y(t)$, three approaches are available to describe the dynamic process

$$\frac{d^{n}y}{dt^{n}}+q_{n-1}\frac{d^{n-1}y}{dt^{n-1}}+\ldots+q_{1}\frac{dy}{dt}+q_{0}y=p_{n-1}\frac{d^{n-1}x}{dt^{n-1}}+p_{n-2}\frac{d^{n-2}x}{dt^{n-2}}+\ldots+p_{1}\frac{dx}{dt}+p_{0}x \tag{4}$$

$$\begin{aligned} \dot{\boldsymbol{u}}(t) &= \vec{\boldsymbol{A}}\boldsymbol{u}(t) + \vec{\boldsymbol{B}}x(t) \\ y(t) &= \vec{\boldsymbol{C}}\boldsymbol{u}(t) \end{aligned} \tag{5}$$

$$y(t) = \int_0^t h(t-\tau)x(\tau)d\tau \tag{6}$$

where n is the order of ordinary differential equation Eq. (4). u(t) is the state vector with dimension $n\times 1$. $\vec{\boldsymbol{A}}$, $\vec{\boldsymbol{B}}$, and $\vec{\boldsymbol{C}}$ are all constant matrices with dimension $n\times n$, $n\times 1$, and $1\times n$. Combining Eq. (4) and Eq. (5),

$$\begin{aligned} \vec{\boldsymbol{A}} &= \begin{bmatrix} -q_{n-1} & -q_{n-1} & \cdots & -q_1 & -q_0 \\ 1 & 0 & \cdots & 0 & 0 \\ 0 & 1 & \cdots & 0 & 0 \\ \vdots & \vdots & \ddots & 0 & 0 \\ 0 & 0 & \cdots & 1 & 0 \end{bmatrix}, \vec{\boldsymbol{B}} = \begin{bmatrix} 1 \\ 0 \\ 0 \\ \vdots \\ 0 \end{bmatrix} \\ \vec{\boldsymbol{C}} &= \begin{bmatrix} p_{n-1} & p_{n-2} & \cdots & p_1 & p_0 \end{bmatrix} \end{aligned} \tag{7}$$

Eq. (6) is the time-domain expression, and it can be transformed to the frequency-domain through the Fourier transformation

$$H(\omega) = \int_0^\infty H(\tau)e^{-i\omega\tau}d\tau = b(\omega) + i\omega\left[a(\omega) - m\right] \tag{8}$$

Then the rational transfer function is established to approximate $H(\omega)$

$$\hat{H}(\omega, \boldsymbol{p}, \boldsymbol{q}) = \frac{p_{n-1}(i\omega)^{n-1} + p_{n-2}(i\omega)^{n-2} + \ldots + p_1 + p_0}{(i\omega)^n + q_{n-1}(i\omega)^{n-1} + \ldots + q_1 + q_0} \tag{9}$$

$\boldsymbol{p}$ and $\boldsymbol{q}$ can be estimated by the least square method. The calculation of $\vec{\boldsymbol{A}}$, $\vec{\boldsymbol{B}}$, and $\vec{\boldsymbol{C}}$ is known as system identification [15]. By using the state-space representation, Eq. (1) is re-written as

$$\begin{aligned} &\left(M + m\right)\ddot{z}(t) = F_{wave}(t) - \vec{\boldsymbol{C}}u(t) - \rho g\pi R^2 z(t) - \left[C + \beta(t)c\right]\dot{z}(t) - Kz(t) \\ &\dot{\boldsymbol{u}}(t) = \vec{\boldsymbol{A}}\boldsymbol{u}(t) + \vec{\boldsymbol{B}}\dot{z}(t) \end{aligned} \tag{10}$$

To implement the control strategy, Eq. (10) is transformed into a first-order differential equation. Define a state vector $\boldsymbol{x} = [\,z, \dot{z}, \boldsymbol{u}^T]^T$ with dimension $(n+2)\times 1$. Then Eq. (10) is re-expressed as

$$\dot{\boldsymbol{x}} = \boldsymbol{\gamma} \cdot \boldsymbol{x} + \boldsymbol{\eta}$$
$$\boldsymbol{\gamma} = \begin{bmatrix} 0 & 1 & \mathbf{0} \\ -\dfrac{\rho g \pi R^2 + K}{M+m} & -\dfrac{C+\beta c}{M+m} & -\dfrac{\vec{\boldsymbol{C}}}{M+m} \\ \mathbf{0} & \vec{\boldsymbol{B}} & \vec{\boldsymbol{A}} \end{bmatrix}, \eta = \begin{bmatrix} 0 \\ \dfrac{F_{wave}}{M+m} \\ \mathbf{0} \end{bmatrix} \tag{11}$$

Based on Eq. (11), the motion of the floater at each time step can be solved with initial condition $\boldsymbol{x}(0) = \mathbf{0}$. Then, the average energy absorption over the time interval [0, T] is given by

$$P = \frac{1}{T}\int_0^T C \cdot \dot{z}(t,\beta)^2 dt \tag{12}$$

III. REAL-TIME LATCHING CONTROL ALGORITHM

A. *Optimal wave energy control*

Assume that the wave forces during the entire time interval [0, T] are already known, the optimal latching control aims to maximize the average energy conversion

$$\max P = \frac{1}{T}\int_0^T C \cdot \dot{z}(t,\beta)^2 dt \tag{13}$$

From a mathematical point of view, it is to maximize P subject to constraint Eq. (11). If the incident wave is regular, it becomes an impedance matching problem and can be solved analytically [5]. Otherwise, the solution is non-causal requiring the information of future control input [16]. Regardless of the incident waves, define a Hamiltonian H:

$$H = C\dot{z}^2 + \boldsymbol{\lambda} \cdot (\boldsymbol{\gamma x} + \boldsymbol{\eta}) \tag{14}$$

$\boldsymbol{\lambda}$ is a state vector with dimension $1\times(n+2)$, which can be regarded as the Lagrange multiplier. According to the Pontryagin's maximum principle, the optimal β is the one maximizing the Hamiltonian at every time step throughout [0, T]. The Hamiltonian is a linear function of β so that β must be the extremal values (0 or 1) to maximize the Hamiltonian. It is easy to find that the Hamiltonian reaches its maximum value on condition that

$$\beta = \begin{cases} 1 & \lambda_2 c\dot{z} < 0 \\ 0 & otherwise \end{cases} \tag{15}$$

Given the random waves within interval [0, T], the time series of floater movement can be calculated. Subsequently, it is next to calculate λ_2 at each time instant and apply the latching control according to the control command. Please note that the sate vector satisfies the following relationships.

$$\begin{aligned} &\dot{\lambda}_i = -\frac{\partial H}{\partial x_i}(t, \mathbf{x}, \beta), i = 1, 2, \ldots, n+2 \\ &\boldsymbol{\lambda}(T) = \mathbf{0} \end{aligned} \tag{16}$$

Eq. (16) cannot be solved numerically like an initial value problem as the final condition is given here. In our study, an iterative process is applied to calculate $\boldsymbol{\lambda}$. Firstly, run the simulation with $\beta(t) = 0$ to obtain the motions free of latching action by integrating Eq. (11) forward from $t = 0$ to $t = T$. Subsequently, determine $\boldsymbol{\lambda}$ by integrating Eq. (16) backwards from $t = T$ to $t = 0$ ($\boldsymbol{\lambda}(T) = \mathbf{0}$ is now an initial condition). Based on Eq. (15), the control sequence $\beta(t)$ is derived. Iterate the process with the updated control sequence until it converges. Please refer to Ref [5] for detailed procedure.

B. Real-time implementation of control

The above procedure outlines the optimal latching control algorithm reported by Babarit and Clement [5]. The optimal latching control is implemented offline assuming that the wave forces over the entire simulation interval are known, which is nearly impossible in real practice. Therefore, the optimal latching control must be modified in practical application.

The receding horizon strategy, resolving the optimization problem at each sampling instant to yield an optimal control sequence (see Fig. 3), is used to implement the latching control online. At time step t_i, optimize the control command β over a prediction horizon interval [t_{i+1}, $t_{i+1}+\Delta t$]. At time step t_{i+1}, apply the control command which has been optimized at the previous step. Please note that only the control command $\beta(t_{i+1})$ is adopted. Recede the prediction horizon interval forward and optimize the control command over [t_{i+2}, $t_{i+2}+\Delta t$]. By repeating this algorithm step by step, control is implemented online throughout the entire interval. This control algorithm is also known as model predictive control [19, 20]. The length of the prediction horizon interval influences control efficiency. In the present study Δt = 2 s is used. It will be clarified in the following part why this value is selected.

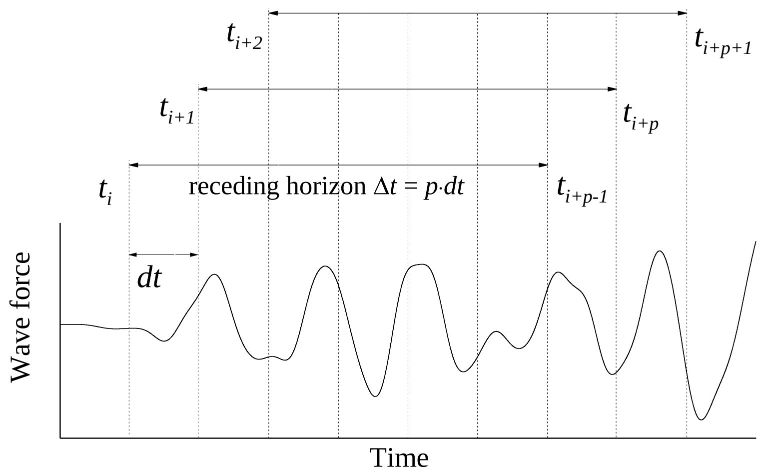

Fig. 3 Receding horizon strategy.

The modifications of the present control algorithm against optimal latching control are summarized as: 1) future wave force is forecasted in the present research; 2) the control command is optimized online over the prediction horizon interval rather than offline over the entire time interval.

C. Short-term wave force prediction

The first order-one variable grey model is used in the present study to forecast the future wave force over the prediction horizon interval by measuring past values. It is worth noting that the wave force is difficult to measure directly. A feasible solution is to monitor the motion of the WEC and link it to the wave force via the WEC dynamic model. Also, the sensor uncertainties are unavoidable. To focus on the scope of the present research, it is assumed that the wave force is measurable and no measurement uncertainties are considered.

The prediction is activated by collecting at least 4 consecutive raw data $\boldsymbol{X}$ in the past. In the present research, the forecasting is based on data over the past 0.5 s. Given that the time discretization is 0.01 s, a total of 50 data points are used for the prediction (n = 50). Moreover, the raw data must be non-negative. A positive offset Q is added to the raw data so that the data will be positive. The offset Q is subsequently deducted from the predicted results at the end of the forecasting process.

$$\boldsymbol{X} = \left(x_1, x_2, ..., x_n\right) + Q, n \geq 4 \tag{17}$$

Get the accumulated series $\boldsymbol{Y}$ from $\boldsymbol{X}$

$$\begin{gathered} \boldsymbol{Y} = \left(y_1, y_2, ..., y_n\right) \\ y_k = \sum_{i=1}^{k} x_i, k = 1, 2, ..., n \end{gathered} \tag{18}$$

Get the background series $\boldsymbol{Z}$

$$\begin{gathered} \boldsymbol{Z} = \left(z_2, z_3, ..., z_n\right) \\ z_k = \left(y_k + y_{k-1}\right)/2 \end{gathered} \tag{19}$$

Set up the grey differential formula

$$x_k + az_k = b, k = 2, 3, .., n \tag{20}$$

and acquire parameters a and b with the least square method

$$\begin{gathered} \begin{bmatrix} a \\ b \end{bmatrix} = \left(A^T A\right)^{-1} A^T B \\ A = \begin{bmatrix} -z_2 & 1 \\ -z_3 & 1 \\ \vdots & \vdots \\ -z_n & 1 \end{bmatrix}, B = \begin{bmatrix} x_2 \\ x_3 \\ \vdots \\ x_n \end{bmatrix} \end{gathered} \tag{21}$$

Establish the first order-one variable grey model to predict the random signal within the interval $[t_{i+1}, t_{i+p}]$

$$\begin{gathered} \hat{x}_{n+p} = \hat{y}_{n+p} - \hat{y}_{n+p-1} - Q \\ \hat{y}_{n+p} = \left(y_1 - \frac{b}{a}\right) e^{-a(n+p-1)} + \frac{b}{a} \end{gathered} \tag{22}$$

where $\hat{x}_{n+p}$ is the predicted data at time step t_{i+p}.

The predictability index in Ref [10] is used here to evaluate the prediction performance of the grey model

$$Er = \frac{\int_{\Delta t}^{T+\Delta t} f^2(t+\Delta t)dt}{\int_0^T \overline{f}^2(t+\Delta t|t)dt} \tag{23}$$

where $\overline{f}(t+\Delta t|t)$ is the prediction of wave force at time instant $t+\Delta t$ forecasted at time instant t; $f(t+\Delta t)$ is the true wave force at time instant $t+\Delta t$. According to the definition, an index around 1 indicates good prediction performance. Fig. 4 demonstrates how the prediction performance varies with the prediction horizon Δt. The index Er deviates away from 1 when Δt increases. Moreover, the prediction accuracy is reduced if too many past data points are used for the prediction, and it justifies why $n = 50$ is employed in the present research. The time series of predicted force $\bar{f}(t+\Delta t|t)$ are plotted in Fig. 5. As shown, the prediction performance becomes worse as the prediction duration Δt increases. Such variation trend is straightforward to understand since long-term future wave forces are more difficult to predict. Since the control command is optimized based on the predicted wave force, whereas the WEC is subject to the true wave force, the control command is not optimal due to the prediction error. The following part will interpret how the prediction error influences the control performance.

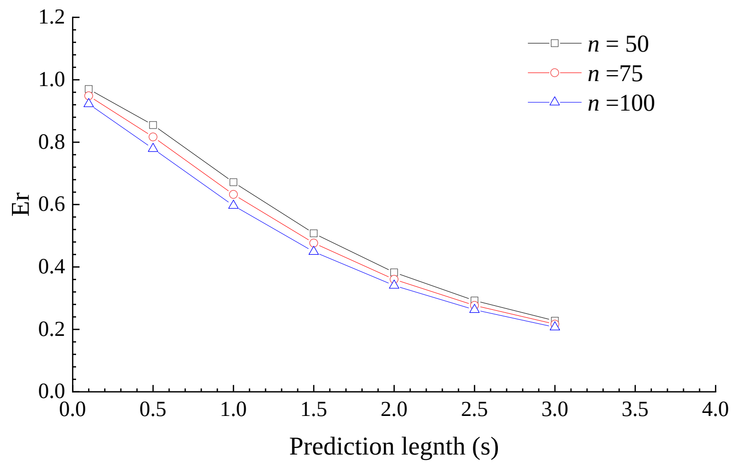

Fig. 4. Effect of prediction length on the prediction performance (Hs = 6m, Top = 13.27s).

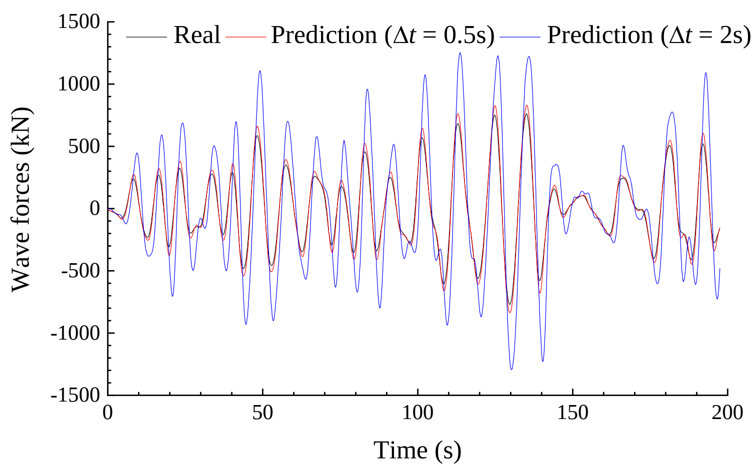

Fig. 5. Time histories of predicted wave forces (Hs = 6m, Tp = 13.27s, n = 50).

IV. VALIDATION

Two aspects of validation are performed, namely the WEC dynamics and the control sequence deduction. The first one aims to ensure that the motions in waves are simulated correctly, which is the basis of control sequence deduction. On condition that the movements are modelled accurately, it subsequently investigates whether the correct control sequence is deduced.

A. WEC dynamics

Firstly, the WEC dynamic model is validated separately in the absence of the latching control. The floater motions in a set of unit regular waves with various periods are simulated. The results are compared with those suggested by frequency-domain hydrodynamic analysis programme WADAM [21]. Please note that the WEC is a linear system without the latching control so that WADAM is applicable here. The PTO system force is modelled with the 'additional damping' and 'additional stiffness' options in WADAM. As displayed in Fig. 6, the agreement between the two simulation tools are good.

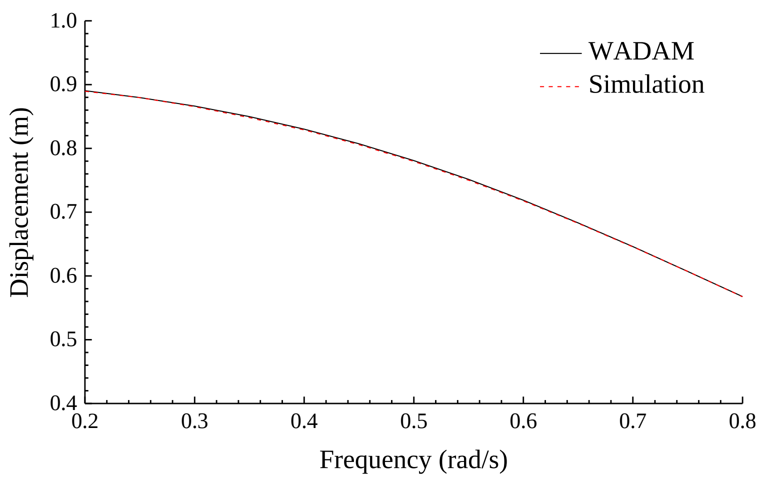

Fig. 6. Floater motions in regular waves.

The experimental data of a cone-cylinder WEC reported by Vantorre et al. [22] are used to validate the present numerical model. The experiment was conducted at a water depth of 1.0 m. Fig. 7. Illustrates the WEC test model. The buoy was a cone-cylinder with a top angle of 90°. The radius was 0.155 m and the draft was 0.218 m. A linear damper was used to represent the PTO system.

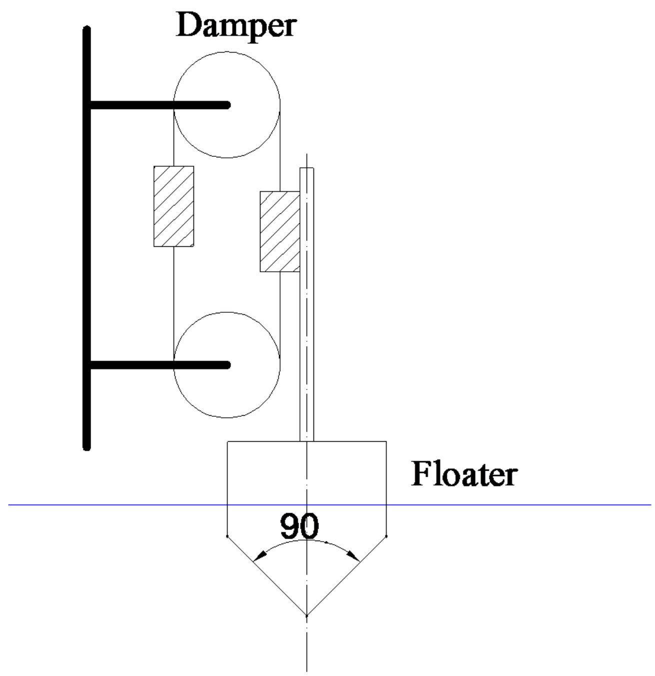

Fig. 7. Configuration of the WEC.

Fig. 8 compares the floater motions in regular wave measured in the model test and predicted by the simulation tool. In general, the agreement between experimental data and simulation results are good.

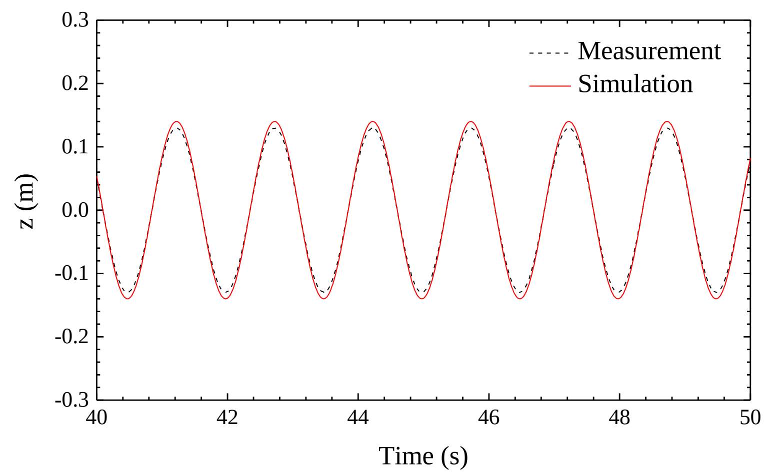

Fig. 8. Floater motion in regular waves. (T = 1.5 s, C = 21.43 kg/s)

B. *control algorithm*

Budal and Falnes [4] found that the energy absorption is maximized when the velocity is in phase with the wave excitation forces. This property is widely accepted as the criterion to validate the latching control. This feature is adopted in the validation of the control algorithm. As shown in Fig. 9, the controlled floater velocity is in phase with the wave force. It indicates the control algorithm is reliable.

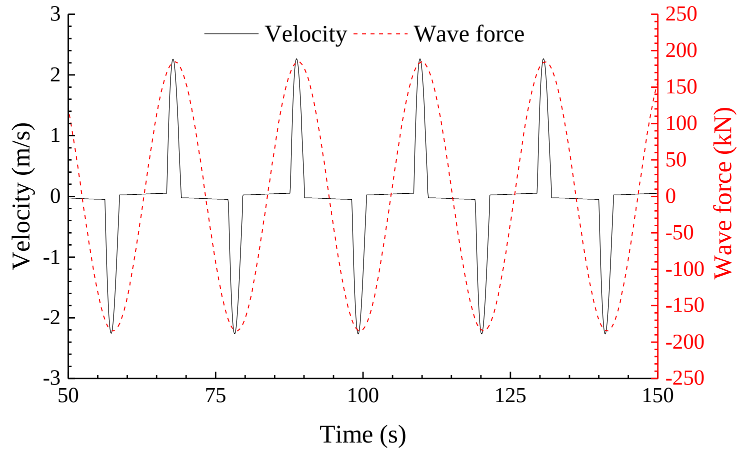

Fig. 9 The phase between velocity and wave force in regular wave, ω = 0.3 rad/s.

V. SIMULATION RESULTS

The joint distribution model of stochastic waves proposed by Li et al. [23] is used to specify the wave spectrum. The distribution model is based on the field measurement at Atlantic from 2001 to 2010. The marginal distribution of significant wave height Hs follows a hybrid lognormal and Weibull distribution

$$f_{H_s}(h)=\begin{cases}\dfrac{1}{\sqrt{2\pi}\sigma_{LHM}h}\cdot\exp\left[-\dfrac{1}{2}\left(\dfrac{\ln(h)-\mu_{LHM}}{\sigma_{LHM}}\right)^2\right] & h\le h_0\\ \dfrac{\alpha_{HM}}{\beta_{HM}}\left(\dfrac{h}{\beta_{HM}}\right)^{\alpha_{HM}-1}\cdot\exp\left[\left(-\dfrac{h}{\beta_{HM}}\right)^{\alpha_{HM}}\right] & h>h_0\end{cases} \tag{24}$$

The conditional distribution of peak period T_p at a given significant wave height follows a lognormal distribution. Detailed values of these parameters can be found in [23].

$$\begin{aligned} f_{T_p|H_s}(t|h)&=\frac{1}{\sqrt{2\pi}\sigma_{LTC}t}\cdot\exp\left[-\frac{1}{2}\left(\frac{\ln(t)-\mu_{LTC}}{\sigma_{LTC}}\right)^2\right]\\ \mu_{LTC}&=c_1+c_2\cdot h^{c_3}\\ \sigma_{LTC}^2&=d_1+d_2\cdot\exp(d_3\cdot h)\end{aligned} \tag{25}$$

A set of significant wave heights are selected artificially, and then the most probable peak periods are determined based on the joint model. The selected random wave conditions are listed in Table I.

Table I
ENVIRONMENTAL CONDITIONS

	Case 1	Case 2	Case 3

H_s (m)	2	4	6
T_p (s)	11.11	12.33	13.27

The total simulation length is 3600 s with the time discretization being 0.01 s. The prediction horizon interval is 2 s. The wave force over the past 0.5 s is used to forecast the incoming wave force.

A. Energy conversion

Fig. 10 compares performances of the WEC in irregular waves with and without the proposed real-time latching control. From the solid red curve representing velocity with the implementation of latching control, it is observed that the floater is locked and released alternately. At the same time, the magnitude of velocity is amplified under the action of latching control. Moreover, one can see that the velocity phase is tuned. The velocity is generally in phase with the wave force due to latching control. The 1-hr average energy harvesting under various wave conditions is illustrated in Fig. 11. The WEC produces up to 40% more power when real-time latching control is implemented..

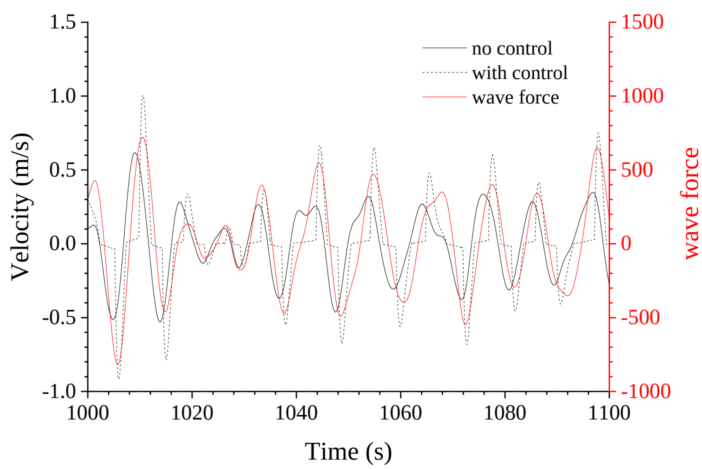

Fig. 10. Responses of the WEC, Case1.

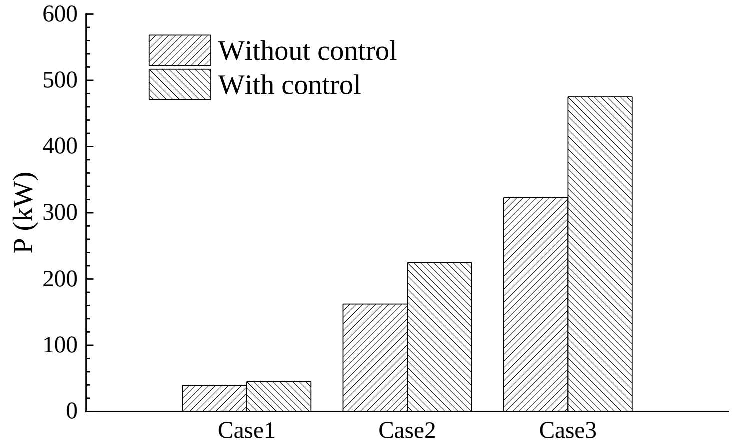

Fig. 11. Average energy harvesting.

B. *Excursion and load of PTO*

One of the significant advantages of latching control against other wave energy control algorithms, e.g. complex conjugate control, is that latching control does not amplify the excursion of PTO. As shown in Table II, the maximum PTO excursion is hardly changed by the implementation of latching control. As well known, the WEC is locked occasionally due to the implementation of latching control and it is found from Fig. 12 that the locking action is applied when PTO excursion is about to reach its maxima. Therefore, PTO excursion is not increased by latching control.

Table II Maximum excursion of the PTO

	With control	Without control
Case1	1.04 m	1.17 m
Case2	2.43 m	2.76 m
Case3	3.53 m	4.12 m

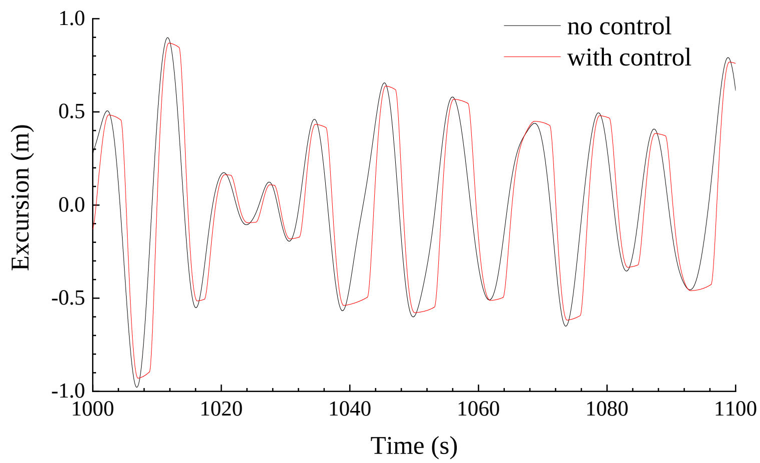

Fig. 12 Time series of PTO movement, Case1.

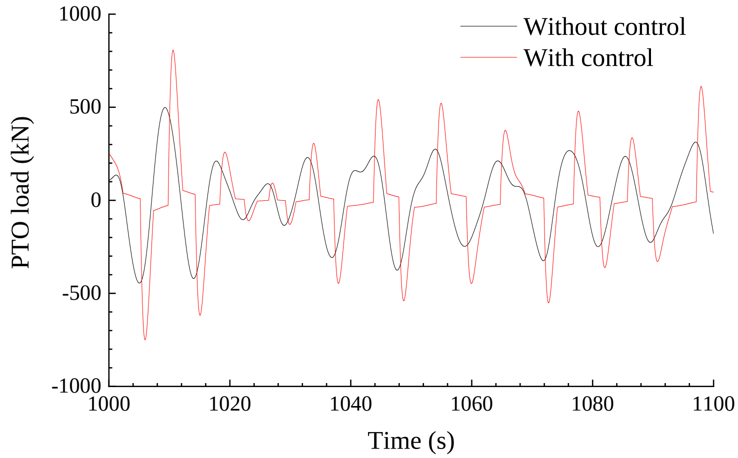

Fig. 13 Time series of PTO load, Case1

However, the PTO load is increased when the latching control is implemented (see Fig. 13). The ultimate PTO load is assessed using up-crossing rate method. It is assumed that the random number of up-crossing are approximated by the Poisson distribution

$$P(y_{\max} \le y_0) = \exp\left(-\int_0^T v^+(y_0,t)dt \right) \tag{26}$$

where $v^+(y_0, t)$ is the up-crossing rate corresponding to level y_0, which denotes the instantaneous frequency of the positive slop crossings of the defined level. In this circumstance, the probability of y_{max} exceeding a specified level y_0 is given by

$$\begin{aligned} &P(y_{\max} > y_0) = 1 - \exp\left(-\hat{v}^+(y_0)T \right) \\ &\hat{v}^+(y_0) = \frac{1}{T}\int_0^T v^+(y_0,t)dt \end{aligned} \tag{27}$$

The mean up-crossing rate $\hat{v}^+(y_0)$ can be easily obtained from the time series of the signal that is going to be analysed. For example, if we have k independent realizations of the random process and let $n_j^+(y_0, T)$ denote the number of up-crossings in realization j, then the sample-based mean up-crossing rate is given by

$$\begin{aligned} &\hat{v}^+(y_o) \approx \overline{v}^+(y_o) \\ &\overline{v}^+(y_o) = \frac{1}{kT}\sum_{j=1}^{k} n_j^+(y_0,T) \end{aligned} \tag{28}$$

Eqs. (26)-(28) give the procedure of estimating the mean up-crossing rate by direct simulation. However, the direct numerical calculation requires extensive time resources to evaluate the statistics of extreme responses that correspond to low probability levels. Therefore, an extrapolation technique is applied to circumvent this obstacle. Based on observations for marine structure, it is concluded that the mean up-crossing rate can be approximated by

$$\bar{v}^{+}(y_o) \approx q \cdot \exp\left\{-a\left(y_0 - b\right)^{c}\right\} \tag{29}$$

Fig. 14 compares the mean up-crossing rate estimated by the direct simulation and the extrapolation technique. As shown, the approximation is satisfactory. Therefore, the extrapolated up-crossing rate is used hereafter to estimate the extreme PTO force. Please refer to Refs [24, 25] for details of the extrapolation technique.

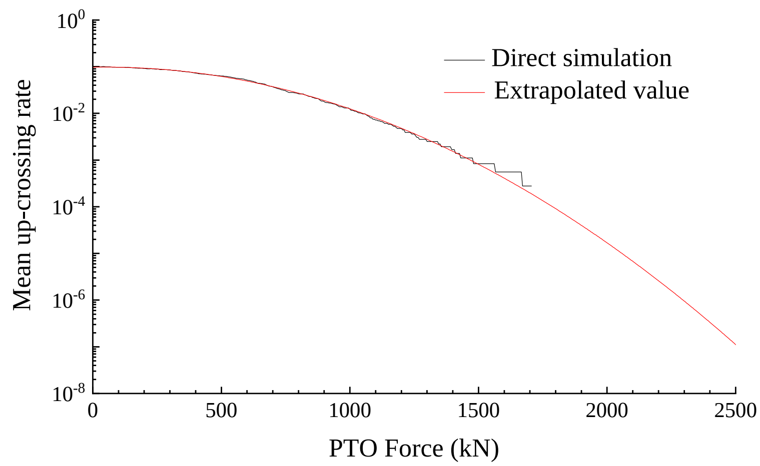

Fig. 14. Extrapolated mean up-crossing rate, Case3, without control.

Fig. 15 plots the extrapolated up-crossing rate of PTO force in the three random wave conditions. Regardless of the wave conditions, the mean up-crossing rate is raised significantly with real-time control. For example, the extrapolated up-crossing rate corresponding to 600 kN is 0.0002 without the real-time control (Case1) and this value hits 0.01 when the real-time control is implemented. Therefore, the extreme PTO force exceeds a certain level more frequently when the point-absorber operates with the real-time control algorithm.

Although the control algorithm is effective in enhancing the energy conversion, the extreme PTO force is amplified substantially in the meanwhile. In the present study, the control algorithm is developed without consideration of any constraint on other aspects, e.g. the maximum velocity, the maximum structural. Such a control algorithm is also known as unconstraint control. If the maximum PTO force is to be considered, the so-called constraint control algorithm should be developed.

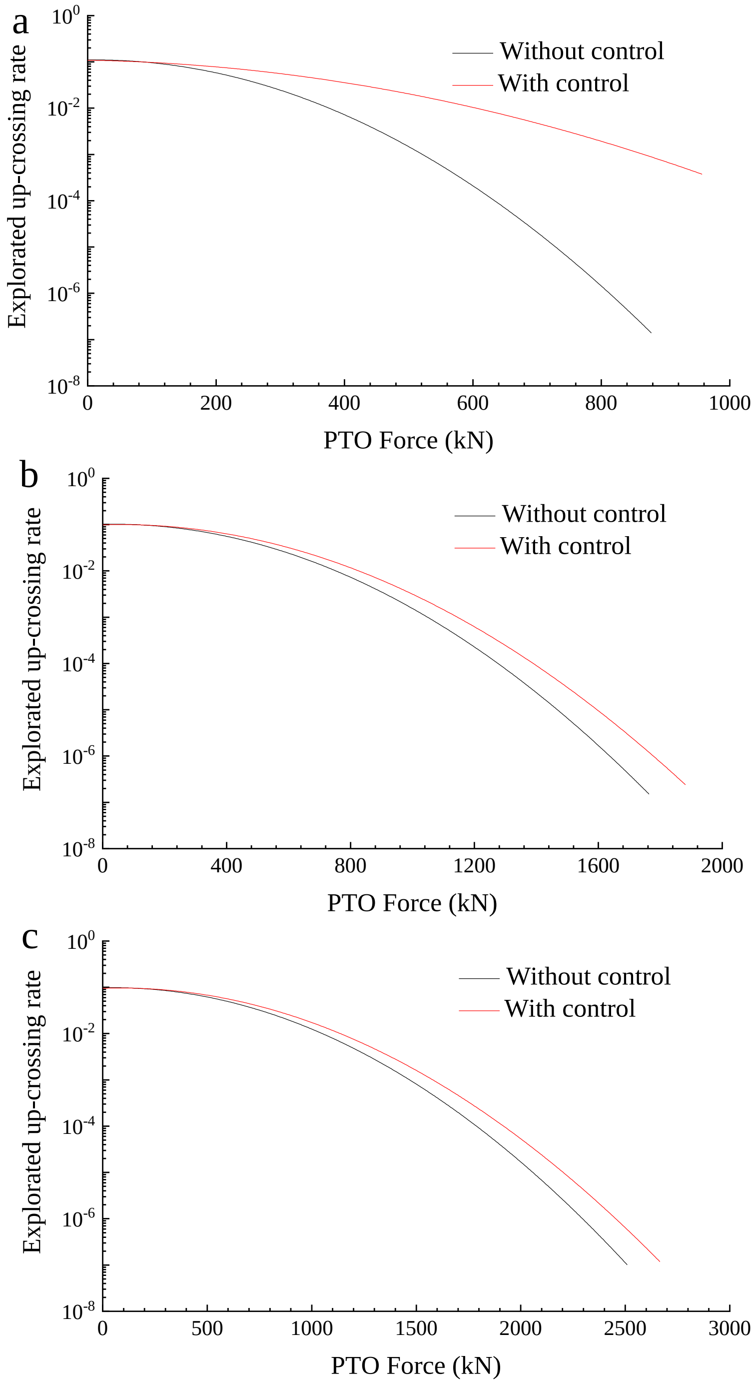

Fig. 15. The extrapolated up-crossing rate of PTO force. (a) Case1; (b) Case2; (c) Case3.

C. Sensitivity of the controller

As summarized in Section III.B, the present control algorithm differs with optimal latching control in two aspects. Firstly, the control command I optimized over the prediction horizon interval. Secondly, the control command is optimized based on the predicted wave force. Table III lists the average energy absorption obtained by using the two control algorithms. Generally, the proposed real-time control is less efficient (15%~20%) than the optimal control due to the two factors. The following part will investigate how the two factors influence the efficiency of the proposed control algorithm.

Table III
AVERAGE ENERGY ABSORPTION ESTIMATED

	Real-time latching control	Optimal latching control
Case1	45 kW	57 kW
Case2	225 kW	263 kW
Case3	475 kW	552 kW

To focus on the effect of prediction horizon interval, it is assumed that the incoming wave forces are already known to eliminate the prediction error. Fig. 16 illustrates how the power extraction varies with the length of prediction horizon interval. Three regions are identified where the energy absorption shows different features. When the control command is optimized over a short horizon interval, the energy absorption remains relatively stable. In this segment, the control action is not effective at all. The performance of WEC is most sensitive to the horizon interval length within the middle segment. In this region, the energy absorption increases significantly with the horizon interval length. As the horizon interval length continues increasing, the energy absorption gradually converges to a fixed level. Any further increase of horizon interval length has a minimal influence on the performance.

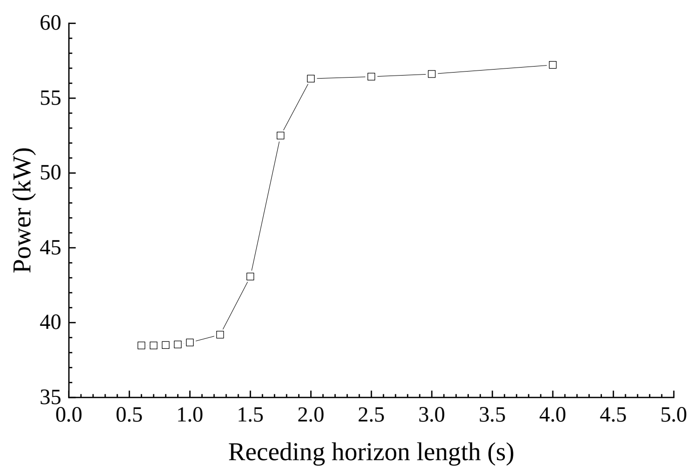

Fig. 16. Variation of power extraction with receding horizon length in the absence of prediction error, Case1.

Fig. 17 illustrates how the horizon interval length influences the control command. When the length is very short, one can see that there is nearly no control action on the PTO system. For most of the moment, the floater is released. It is why the energy capture performance is hardly improved. As the length increases, the floater is latched more frequently, indicating that the control action grows stronger. As a result, energy absorption increases gradually. When the horizon interval is sufficiently long, the control command in Fig. 17 (c) and Fig. 17 (d) match well with each other. Consequently, the curve in Fig. 16 converges to a fixed level at the tail region.

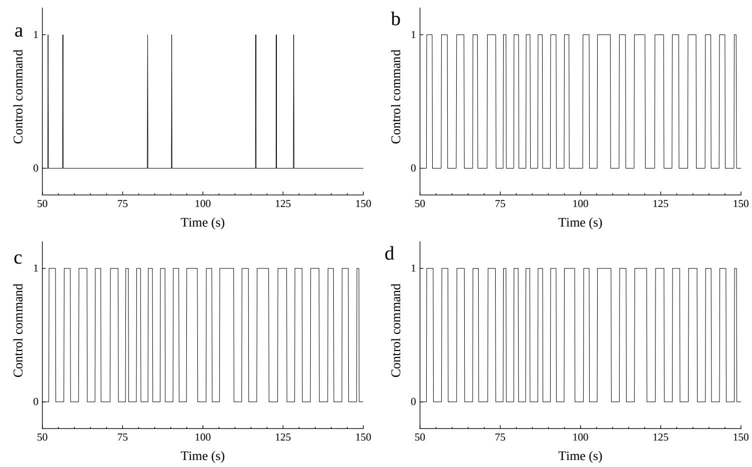

Fig. 17. Control command with various receding horizon lengths, Case1. (a) Δt = 1.0 s; (b) Δt = 2.0 s; (c) Δt = 3.0 s; (d) Δt = 4.0 s.

The second factor influencing the control efficiency is the precision of the prediction model. Fig. 18 demonstrates the prediction error effect on the energy conversion, in which the prediction length is 2 s. The level of prediction error is tuned by adjusting *n* (please refer to Eq. (17) for the definition of *n*). As shown, the control efficiency increases when the prediction error is reduced. The control commands with different levels of prediction error are plotted in Fig. 19. Due to the prediction error, the WEC is locked inappropriately, leading to the reduction of energy conversion.

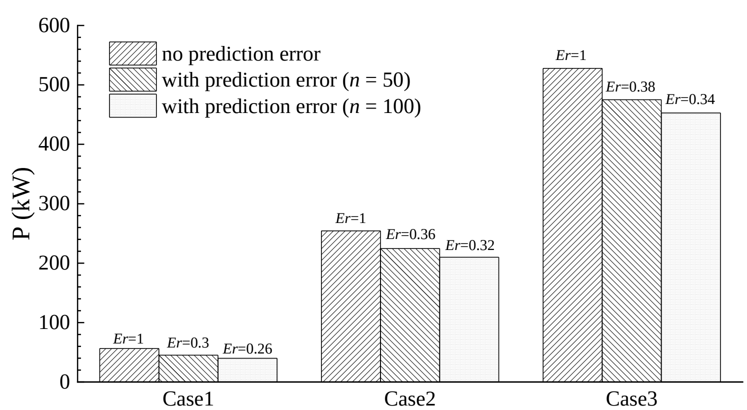

Fig. 18. Effect of prediction error on energy conversion. Δt = 2 s.

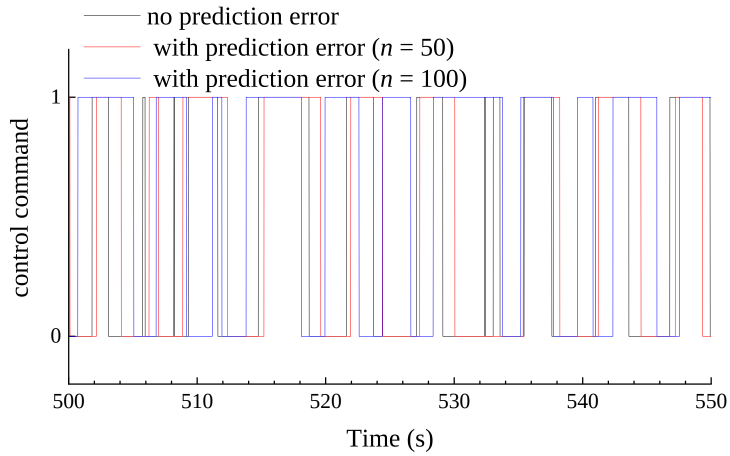

Fig. 19. Effect of prediction error on control command. Case1, $\Delta t = 2$ s.

A long prediction horizon interval is always beneficial to the energy absorption in the absence of prediction error. However, the prediction error harms the energy conversion and it accumulates over the prediction horizon interval (see Fig. 4). It is a trade-off between forecasting length and forecasting precision. Fig. 20 illustrates how the energy conversion varies with the forecasting length when the future wave forces are predicted using the grey model. When a short forecasting length is employed, the forecasting error is limited and thereby it has a minimal influence on the performance of the WEC. As pointed out before, a larger forecasting length is beneficial to energy absorption. Consequently, the WEC harvests more energy when the forecasting length is increased to 2 s even if the forecasting error grows in the meanwhile. In the case of larger forecasting error, the discrepancies become more notable. Therefore, a moderate forecasting length is recommended in practical application. For the present study, $\Delta t = 2$ s is the optimal choice. Nevertheless, this value may vary with the wave force prediction model employed.

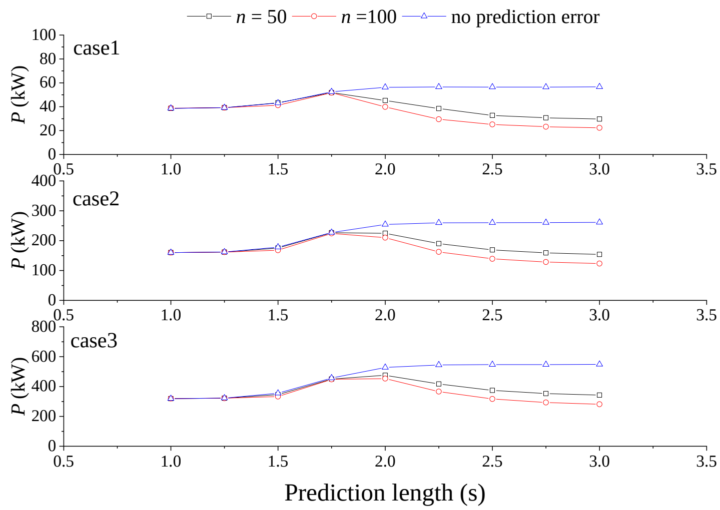

Fig. 20. Influence of prediction deviation.

As presented in Section III.C, the forecasting error can be represented by Eq. (23) quantitively. Fig. 21 plots how the power extraction varies with the forecasting error *Er*. It is observed that the power extraction begins to drop when *Er* is lower than 0.35. Therefore, it is recommended that the forecasting error should not exceed this threshold for application in wave energy control.

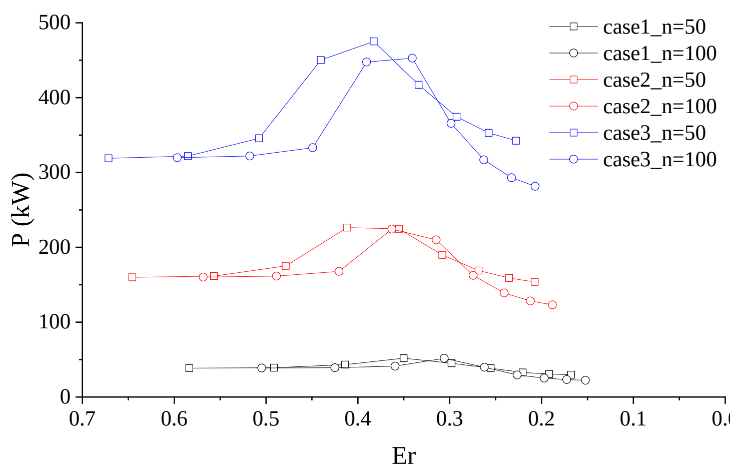

Fig. 21 Variation trend of power extraction with respect to forecasting error Er.

VI. CONCLUSION

A real-time latching control algorithm based on wave force prediction is developed. The wave forces over the prediction interval are forecasted with the grey model and then the control command is optimized based on the forecasted future wave force. By updating the wave force prediction and the control command optimization at each time instant, the control is implemented online.

For the random wave conditions considered in this study, the energy absorption can be increased by more than 40% with the application of real-time latching control. The extreme PTO force is increased substantially with the real-time control algorithm. In the present study, the control algorithm is developed without consideration of the maximum PTO force so that it is unconstraint control.

A longer receding horizon length is beneficial to the energy absorption in the absence of prediction deviation. The energy absorption varies hardly with the receding horizon length initially. When the receding horizon length is very short, the deduced control action has little influence on energy absorption. Afterwards, it becomes sensitive to the change of horizon and increases significantly with the horizon. When the receding horizon length is long enough, the energy absorption converges gradually.

The influence of prediction deviation on the energy capture performance is investigated. It is shown that energy absorption is reduced as a result of the prediction deviation. As the prediction deviation accumulates over the receding horizon, a long receding horizon is not always beneficial to the energy capture. It is recommended that the prediction error *Er* should not be lower than 0.35 for application in wave energy control.

ACKNOWLEDGEMENT

This work is funded by State Key Laboratory of Hydraulic Engineering Simulation and Safety, Tianjin University (HESS-1919) and State Key Laboratory of Coastal and Offshore Engineering, Dalian University of Technology (LP1908). The second author gratefully acknowledges the supports of the Fund of State Key Laboratory of Ocean Engineering (GKZD010074) and Shanghai Sailing Program (18YF1411500).

REFERENCES

[1] ExxonMobile, "Outlook for Energy: A View to 2040," 2017.
[2] X. T. Zhang, X. L. Tian, L. F. Xiao, X. Li, and L. F. Chen, "Application of an adaptive bistable power capture mechanism to a point absorber wave energy converter", *Appl Energ*, vol. 228, pp. 450-467, Oct 15 2018, doi: 10.1016/j.apenergy.2018.06.100.
[3] W. A. Sheng and A. Lewis, "Power Takeoff Optimization to Maximize Wave Energy Conversions for Oscillating Water Column Devices,", *Ieee J Oceanic Eng*, vol. 43, no. 1, pp. 36-47, Jan 2018, doi: 10.1109/Joe.2016.2644144.

[4] K. Budal and J. Falnes, *Interacting point absorbers with controlled motion, in Power from Sea Waves*. BM Count, Academic Press, 1980.
[5] A. Babarit and A. H. Clement, "Optimal latching control of a wave energy device in regular and irregular waves,", *Appl Ocean Res*, vol. 28, no. 2, pp. 77-91, Apr 2006, doi: 10.1016/j.apor.2006.05.002.
[6] J. C. C. Henriques, L. M. C. Gato, A. F. O. Falcao, E. Robles, and F. X. Fay, "Latching control of a floating oscillating-water-column wave energy converter,", *Renew Energ*, vol. 90, pp. 229-241, May 2016, doi: 10.1016/j.renene.2015.12.065.
[7] A. Babarit, G. Duclos, and A. H. Clement, "Comparison of latching control strategies for a heaving wave energy device in random sea,", *Appl Ocean Res*, vol. 26, no. 5, pp. 227-238, Jul 2004, doi: 10.1016/j.apor.2005.05.003.
[8] J. R. Halliday, D. G. Dorrell, and A. R. Wood, "An application of the Fast Fourier Transform to the short-term prediction of sea wave behaviour,", *Renew Energ*, vol. 36, no. 6, pp. 1685-1692, Jun 2011, doi: 10.1016/j.renene.2010.11.035.
[9] D. Q. Truong and K. K. Ahn, "Wave prediction based on a modified grey model MGM(1,1) for real-time control of wave energy converters in irregular waves,", *Renew Energ*, vol. 43, pp. 242-255, Jul 2012, doi: 10.1016/j.renene.2011.11.047.
[10] F. Fusco and J. V. Ringwood, "Short-Term Wave Forecasting for Real-Time Control of Wave Energy Converters,", *IEEE T Sustain Energ*, vol. 1, no. 2, pp. 99-106, Jul 2010, doi: 10.1109/Tste.2010.2047414.
[11] M. P. Schoen, J. Hals, and T. Moan, "Wave Prediction and Robust Control of Heaving Wave Energy Devices for Irregular Waves,", *Ieee T Energy Conver*, vol. 26, no. 2, pp. 627-638, Jun 2011, doi: 10.1109/Tec.2010.2101075.
[12] G. Li, G. Weiss, M. Mueller, S. Townley, and M. R. Belmont, "Wave energy converter control by wave prediction and dynamic programming,", *Renew Energ*, vol. 48, pp. 392-403, Dec 2012, doi: 10.1016/j.renene.2012.05.003.
[13] P. C. Vicente, A. F. O. Falcao, and P. A. P. Justino, "Nonlinear dynamics of a tightly moored point-absorber wave energy converter,", *Ocean Eng*, vol. 59, pp. 20-36, Feb 1 2013, doi: 10.1016/j.oceaneng.2012.12.008.
[14] X. T. Zhang, J. M. Yang, W. H. Zhao, and L. F. Xiao, "Effects of wave excitation force prediction deviations on the discrete control performance of an oscillating wave energy converter,", *Ships Offshore Struc*, vol. 11, no. 4, pp. 351-368, 2016, doi: 10.1080/17445302.2014.998858.
[15] R. Taghipour, T. Perez, and T. Moan, "Hybrid frequency-time domain models for dynamic response analysis of marine structures,", *Ocean Eng*, vol. 35, no. 7, pp. 685-705, May 2008, doi: 10.1016/j.oceaneng.2007.11.002.
[16] J. Falnes, *Ocean waves and oscillating systems: linear interactions including wave-energy extraction*. Cambridge university press, 2002.
[17] L. Li, Z. M. Yuan, and Y. Gao, "Maximization of energy absorption for a wave energy converter using the deep machine learning,", *Energy*, vol. 165, pp. 340-349, Dec 15 2018, doi: 10.1616/j.energy.2018.09.093.
[18] L. Li, Z. M. Yuan, Y. Gao, and X. S. Zhang, "Wave Force Prediction Effect on the Energy Absorption of a Wave Energy Converter With Real-Time Control,", *IEEE T Sustain Energ*, vol. 10, no. 2, pp. 615-624, Apr 2019, doi: 10.1109/Tste.2018.2841886.
[19] G. Li and M. R. Belmont, "Model predictive control of sea wave energy converters - Part I: A convex approach for the case of a single device,", *Renew Energ*, vol. 69, pp. 453-463, Sep 2014, doi: 10.1016/j.renene.2014.03.070.
[20] G. Li and M. R. Belmont, "Model predictive control of sea wave energy converters - Part II: The case of an array of devices,", *Renew Energ*, vol. 68, pp. 540-549, Aug 2014, doi: 10.1016/j.renene.2014.02.028.

[21] DNV, "WADAM—Wave Analysis by Diffraction and Morison Theory," in "SESAM user's manual, Høvik," 1994.
[22] M. Vantorre, R. Banasiak, and R. Verhoeven, "Modelling of hydraulic performance and wave energy extraction by a point absorber in heave,", *Appl Ocean Res,* vol. 26, no. 1-2, pp. 61-72, Feb-Apr 2004, doi: 10.1016/j.apor.2004.08.002.
[23] L. Li, Z. Gao, and T. Moan, "Joint Distribution of Environmental Condition at Five European Offshore Sites for Design of Combined Wind and Wave Energy Devices,", *J Offshore Mech Arct,* vol. 137, no. 3, p. 031901, Jun 2015, doi: 10.1115/1.4029842.
[24] Z. S. Cheng, H. A. Madsen, W. Chai, Z. Gao, and T. Moan, "A comparison of extreme structural responses and fatigue damage of semi-submersible type floating horizontal and vertical axis wind turbines,", *Renew Energ,* vol. 108, pp. 207-219, Aug 2017, doi: 10.1016/j.renene.2017.02.067.
[25] L. Li, Z. S. Cheng, Z. M. Yuan, and Y. Gao, "Short-term extreme response and fatigue damage of an integrated offshore renewable energy system,", *Renew Energ,* vol. 126, pp. 617-629, Oct 2018, doi: 10.1016/j.renene.2018.03.087.

Liang Li received his B.S. and M.Sc. degrees from Shanghai Jiao Tong University, and Ph.D. degree from University of Strathclyde. He is currently working in University of Strathclyde. His research topic is mainly relating renewable energy, with a focus on the wave energy converter control.

Hongdong Wang received the B.E., M.E., and Ph.D. degrees from Shanghai Jiao Tong University, Shanghai, China in 2011, 2014 and 2016, respectively. He is now the lecturer with the School of Naval Architecture, Ocean and Civil Engineering, Shanghai Jiao Tong University, China. His research interests include control and testing of marine operation.

Yan Gao received her B.S. and M.Sc. degrees from Shanghai Jiao Tong University. Now, she is working towards her Ph.D. degree in University of Strathclyde. Her research interest mainly focuses on structure-fluid coupling.